2022 IEEE/RSJ International Conference on Intelligent Robots and Systems (IROS)
October 23-27, 2022, Kyoto, Japan

Improved Zero Step Push Recovery with a Unified Reduced Order Model of Standing Balance

Thomas Huckell[1] and Amy R. Wu[1*]

Abstract— **Standing balance for legged robots can be achieved through regulating the center of pressure (ankle strategy), the angular momentum about the center of mass (hip strategy), and the magnitude of ground reaction force (variable height strategy). Prevalent reduced order models used to model legged robots at most only capture two of these strategies, and the contribution of the three available strategies is unclear. We propose a unified reduced order model that includes all three standing balance strategies and compared push recovery simulations of the unified model against existing balancing models using a nonlinear model predictive controller. We also developed a full body controller for a simple one legged balancing robot that tracked control from the reduced order models. For both the reduced order model and robot simulations, we found that the unified model could recover successfully from the largest pushes and yielded the smallest center of mass excursions. Between the hip and variable height strategies, the hip had the greatest effect on improving performance. Our results suggest that successful implementation of a unified reduced order model on physical robots would enable a simplified controller that takes advantage of available balancing strategies as needed to recover from larger push disturbances than feasible before.**

I. Introduction

Legged robots require active balancing to remain stable in the presence of unintended disturbances. Robot balancing strategies have been classified into four distinct strategies – ankle, hip, variable height, and stepping [1]. The ankle strategy uses ankle torques to regulate the position of the center of pressure (CoP) within the polygon of support created by foot contact with the ground. The hip strategy utilizes upper body dynamics to generate angular momentum about the center of mass (CoM) to produce restoring shear forces at the base of support. The variable height strategy utilizes the vertical dynamics of the CoM to generate increased ground reaction forces. The stepping strategy regulates the polygon of support by adjusting the foot contact point.

Previous work in humanoid robot control have sought to unify multiple balance strategies into a single model for push recovery. Some models switch among balance controllers that represent each strategy with some decision criterion [2] or through changing optimization weights [3]. Multiple strategies have also been achieved through a single controller (e.g. model predictive control [4], [5]) or optimization criterion [6]. While these studies have primarily focused on the ankle, hip, and stepping strategies, McGreavy et al. included the variable height strategy in their model, which was developed by fitting their controllers to human responses to perturbations [1].

The standing balance strategies have been approximated by reduced order models that simplify the complexity of high dimensional, full body systems while still encapsulating the key dynamics characteristics of robot CoM motion [7]. One prominent reduced order model is the linear inverted pendulum (LIP) [8]. This model reduces balancing to the control of the CoP within the polygon of support, approximating the ankle strategy [2]. While reduced order models may simplify the control of legged robots, they might also reduce robot performance and capabilities by restricting its motion. The CoM trajectory and the angular momentum about CoM in the LIP model are constrained and cannot utilize the benefits of the hip and variable height strategies. Several extensions of the LIP model have been developed to relax these constraints and include additional balancing strategies. The linear inverted pendulum plus flywheel (LIPPFW) model includes angular momentum about the CoM and approximates a combined ankle and hip strategy [9]. A combined ankle and variable height strategy can be approximated by the variable height inverted pendulum (VHIP) model which relaxes the restriction on the vertical CoM trajectory [10]. Reduced order models are useful for robot control, but current reduced order models approximate at most two of the available standing strategies [2], [4]. It is unclear how the variable height strategy contributes to overall standing balance and how its relative contributions with the ankle and hip strategies change with perturbation magnitude.

Here, we combined the three standing balance strategies into one unified reduced order model we call the variable height inverted pendulum plus flywheel (VHIPPFW) model. To evaluate our unified model against previous reduced order models (LIP, LIPPFW, VHIP), we compared the push recovery performance of all four reduced order models over a range of push disturbances using a nonlinear model predictive controller (NMPC). In response to the perturbations, we determined the relative contributions of the ankle, hip, and variable height strategies within our model. We then applied the NMPC controller based on each reduced order model in the simulation of a simple one legged robot as a step towards their practical implementation as a standing balance controller.

II. Methods

We explored the zero step push recovery of reduced order models and later implemented them to control a simple one legged balancing robot in simulation. We used a NMPC

[1]Thomas Huckell and Amy R. Wu are with the Department of Mechanical and Materials Engineering and Ingenuity Labs Research Institute, Queen's University, Kingston, Ontario, K7L 3N6, Canada thomas.huckell@queensu.ca, amy.wu@queensu.ca.

2022 IEEE/RSJ International Conference on Intelligent Robots and Systems (IROS) | 978-1-6654-7927-1/22/$31.00 ©2022 IEEE | DOI: 10.1109/IROS47612.2022.9981193

controller based on each reduced order model to generate the control needed to recover from push disturbances. We then developed a simple one legged robot to use the NMPC constructed for each reduced order model to generate motion objectives for the robot to follow. This section details the reduced order models used by the NMPC, the NMPC controller, the simple one legged robot model, and the full body controller that generated the joint torques for the robot from the reduced order NMPC.

A. Reduced Order Models

The reduced order models used in this study include the LIP, LIPPFW, VHIP and VHIPPFW (Fig. 1).

1) Linear Inverted Pendulum (LIP): The LIP model (Fig. 1a) consists of a point mass supported by a massless leg and assumes that there is no angular momentum and no change in angular momentum to the system. Furthermore, the CoM position is constrained to a planar trajectory, and often this trajectory is a constant height [8], [11]. Under these constraints, the ground reaction force is located at the CoP with a line of action passing through the CoM such that there is no moment about the CoM. These assumptions result in a simple linear expression that has been used in walking pattern generation and control [12]. In standing balance, the model is controlled through placing the CoP within the support polygon. The LIP sagittal dynamics are given by

$$\ddot{x} = \frac{g}{z_0}(x - x_c) \tag{1}$$

where x is the position of the CoM in the sagittal plane, z_0 is the CoM height, x_c is the location of the CoP which is constrained to be within the support polygon $\delta^- \leq x_c \leq \delta^+$, and g is the gravitational acceleration. In this model, the state is $X = [x, \dot{x}]^T$ and control is $U = x_c$

2) Linear Inverted Pendulum Plus Flywheel (LIPPFW): Humans use their torso and arms to generate angular momentum which has been shown to play a significant role in balance [13], especially to recover from large perturbations [14], [15]. The LIPPFW model (Fig. 1b) seeks to capture these benefits by including a flywheel with inertial properties centered at the CoM of the LIP model. The sagittal and flywheel dynamics of the LIPPFW model are given by

$$\ddot{x} = \frac{g}{z_0}(x - x_c) - \frac{\tau}{m z_0} \tag{2}$$

$$J\ddot{\theta} = \tau \tag{3}$$

where τ is the torque about the CoM in the sagittal plane, θ is the flywheel angle which is constrained by the joint limits $\theta_{\max} \leq \theta \leq \theta_{\min}$, and J is the inertia of the flywheel. The state and control of this model is $X = [x, \theta, \dot{x}, \dot{\theta}]^T$ and $U = [x_c, \tau]^T$, respectively.

3) Variable Height Inverted Pendulum (VHIP): Vertical dynamics can improve disturbance rejection and increase the horizontal force that can be applied to the CoM to further extend the region of stability over the LIP [10], [16], [17]. The challenge with releasing the constraint on vertical height is the nonlinearity of the dynamics. Assuming no change in angular momentum, the ground reaction force's line of action passes from the CoP through the CoM (Fig. 1c), resulting in the sagittal plane dynamics given by

$$\ddot{x} = \frac{(g + \ddot{z})}{z}(x - x_c) \tag{4}$$

where z is the vertical position of the CoM bounded by $z_{\min} \leq z \leq z_{\max}$. The state and control for this model is $X = [x, z, \dot{x}, \dot{z}]^T$ and $U = [x_c, \ddot{z}]$, respectively.

4) Variable Height Inverted Pendulum Plus Flywheel (VHIPPFW): We developed this unified standing balance model VHIPPFW (Fig. 1d) to utilize the ankle, hip and variable height balancing strategies in one reduced order model. The sagittal dynamics are given by (5) with the same flywheel dynamics as (3).

$$\ddot{x} = \frac{(g + \ddot{z})}{z}(x - x_c) - \frac{\tau}{mz} \tag{5}$$

For this model, the state is $X = [x, \theta, z, \dot{x}, \dot{\theta}, \dot{z}]^T$, and the control is $U = [x_c, \tau, \ddot{z}]^T$.

B. Model Parameters

The reduced order model parameters were chosen to approximate an average human [18] with specified state and control values at rest and their respective limits (summarized in Table I). We used a mass of 70 kg, upper body inertia about the CoM of 8 kg-m^2, upper limit of the base of support δ^+ of 0.2 m, and a maximum flywheel torque $\tau_{\max}$ of 100 N-m. For the variable height strategy, we used a $\ddot{z}$ limit similar to that used on the Valkyrie humanoid robot [10].

TABLE I: State and control bounds for the reduced order models. The min and max x_c are δ^- and δ^+, respectively.

Symbol	Description (units)	Rest	Min	Max
θ	flywheel angle (rad)	0	-0.5	0.5
z	CoM height (m)	0.7896	0.67	0.886
x_c	CoP position (m)	0	-0.1	0.2
τ	flywheel torque (Nm)	0	-100	100
$\ddot{z}$	vertical acceleration (m/s^2)	0	-3	3

C. Nonlinear Model Predictive Controller (NMPC)

Due to the nonlinear nature of the reduced order model dynamics when the constant height constraint is relaxed, a nonlinear model predictive controller (NMPC) was used for balance control. The NMPC recursively solves discrete time finite horizon optimization problems, minimizing an objective function subject to the constraints of system dynamics and state and control limits. Our objective function penalized deviations from the reference rest state along with the added cost of control and control rate.

$$\begin{aligned} \min_{X,U} \quad & \sum_{i=2}^{P} T(\tilde{X}_i^T Q \tilde{X}_i + U_i^T R U_i + k \Delta U_i^T R \Delta U_i) \\ \text{subject to} \quad & X_{i+1} = f(X_i, U_i), \quad i = 1, ..., P-1 \\ & X_{\min} \leq X_i \leq X_{\max} \quad i = 1, ..., P \\ & U_{\min} \leq U_i \leq U_{\max} \quad i = 1, ..., P \end{aligned} \tag{6}$$

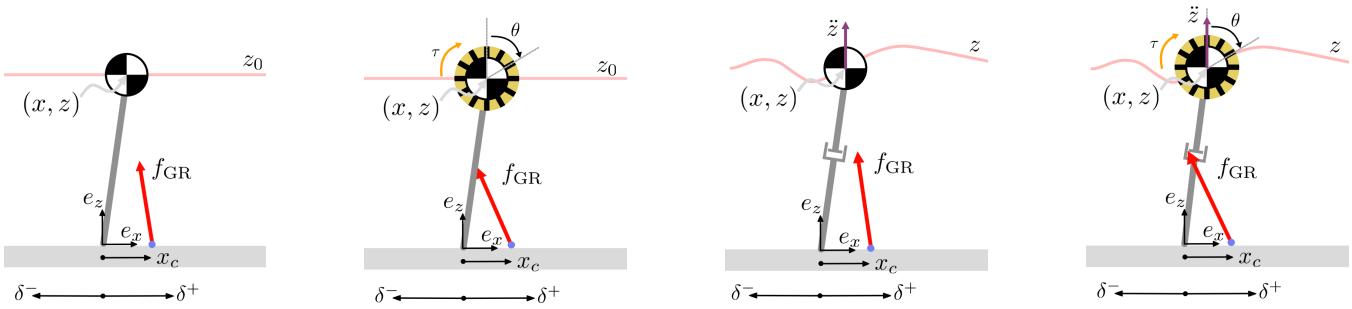

(a) LIP (b) LIPPFW (c) VHIP (d) VHIPPFW

Fig. 1: Reduced order models for balance: (a) the linear inverted pendulum (LIP), the linear inverted pendulum plus flywheel (LIPPFW), (c) the variable height inverted pendulum (VHIP), and (d) variable height inverted pendulum plus flywheel model (VHIPPFW).

TABLE II: Weighting factors for elements of state

State	Weighting Factor
x	$3.5/\delta^{+2}$
θ	$0.9/\theta^2_{\max}$
z	$0.6/z^2_{\max}$
$\dot{x}$	$12/0.45^2$
$\dot{\theta}$	$0.81/\dot{\theta}^2_{\max}$
$\dot{z}$	$0.36/\dot{z}^2_{\max}$

TABLE III: Weighting factors for elements of control

Control	Weighting Factor
x_c	$1/\delta^{+2}$
τ	$0.9/\tau^2_{\max}$
$\ddot{z}$	$0.5/\ddot{z}^2_{\max}$
k	2.5

where $_i$ indicates i^{th} element in the prediction horizon P, $\tilde{X}_i = X_i - X_0$ is the state deviation from rest position, Q and R are diagonal weighting matrices with weighting factors along the diagonal, k is the control rate weighting factor to penalize oscillatory control responses, $\Delta U_i = U_{i+1} - U_i$ with $\Delta U_P = 0$, $f(X_i, U_i)$ is the discretized model dynamics, and $X_{\min}$, $X_{\max}$, $U_{\min}$, and $U_{\max}$ are limits on the admissible state and control set (Table I). The weighting factors were designed to normalize the elements of the state and control to their upper bounds such that differences in magnitude do not influence the optimization. Due to the short prediction horizon favoring the ankle strategy, the weighting factors were manually scaled such that for LIPPFW and VHIP, the NMPC utilized hip and variable height strategies and produced control efforts proportional to disturbance magnitude, building to a maximal control effort similar to the bang-bang control schemes in [9] and [10] at the limits of stability. Each element of the state and control has a unique weighting factor, and the size and entries of Q and R change depending on the reduced order model used (Table II and III).

We used the *nlmpc* function (MathWorks, Natick, USA) to solve the NMPC problem with $P = 14$ and a sampling time of 0.05 s. These parameters were chosen to balance computational complexity and response time to perturbations. For each NMPC, we used the model dynamics of the respective reduced order model, and set the reference trajectory to be the rest state and control target as zero for upright standing.

D. Simple One Legged Balancing Robot

To test practical implementation of the NMPC controllers of the reduced order models in standing push recovery, we implemented the controller on a simple one legged robot model. The one legged balancing robot was constructed in Simscape Multibody (Mathworks, Natick, USA) and constrained to the sagittal plane. The robot has a total mass of 70 kg and is 1.38 m tall when fully upright. It consisted of torso, thigh, shank and foot segments connected with actuated revolute joints (Fig. 2). The robot was constructed to approximate human anthropometric parameters (from [19]) to gain insights into human balancing and adult-size humanoid legged robots (Table IV).

The mass within each segment was uniformly distributed with inertial properties based on its geometry. The torso inertia was changed to match the inertia of the upper body segment with respect to the COM from [18]. With respect to the ankle joint, the support polygon limits were $[\delta^-, \delta^+] = [-0.1, 0.2]$.

To model the contact between the foot and support surface, we added 3D sphere-to-plane contact points to each foot corner using the Simscape Multibody Contact Forces Library [20]. Except for a lowered velocity threshold of 0.025 m/s to prevent slipping, we used a linear force model and a continuous friction model with contact model parameters from [21]. We measured the CoP as the weighted average position of normal forces from the contact points.

The robot is at rest at the start and end of the simulation. The initial position was set such that the hip joint is at the desired height of z_0, and the CoM of the robot is projected over the ankle joint. The trunk is upright, and all velocities are zero. The joint torques were set to the torques required to counteract the gravitational forces. Although not representative of upright human standing, the resulting crouched posture (Fig. 2) was necessary to employ the variable height strategy with the knee joint.

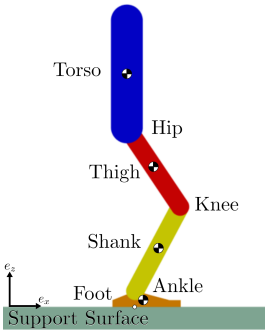

Fig. 2: Simple one legged balancing robot.

TABLE IV: Robot anthropometric parameters

Segment	Mass [kg]	Length [m]	Inertia [kg-m^2]
Torso	47.67	0.47	5.37
Thigh	14.0	0.42	0.28
Shank	6.3	0.42	0.13
Foot[1]	2.03	0.30	0.011

[1]Ankle joint is 0.07 m from the ground.

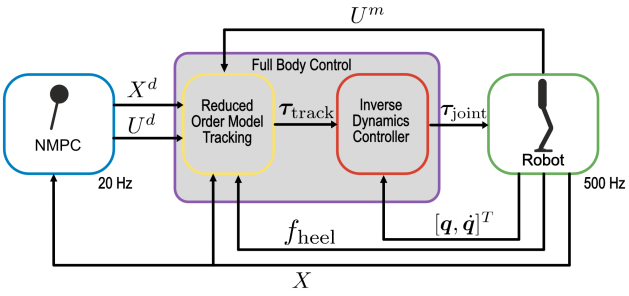

Fig. 3: Block diagram for the balancing robot controller. The NMPC block passes the controls of the reduced order model to the full body controller. The full body controller produces joint torques to track the model and the torques to compensate for the effects of gravity and the torques induced by joint velocities and estimated accelerations. $[q, \dot{q}]^T$ is joint position and velocities, and f_{heel} is the normal heel force.

E. Full Body Control

A full body controller generated joint torques τ_{joint} for the one legged robot based on the desired control and state of the reduced order models. It consisted of a reduced order model tracking controller and an inverse dynamics controller (Fig. 3). The reduced order model tracking controller converted the NMPC controls to the corrective joint torques τ_{track} required to track the reduced order model. The corrective torque is then fed to an inverse dynamics controller (utilizing *inverseDynamics* function, Mathworks, Natick, USA) to add the torques needed to compensate for the torques induced by gravity and by the joint velocities and estimated accelerations given the current state of the robot and its dynamics.

The reduced order model tracking controller used the hip, knee, and ankle as the primary means of regulating the flywheel torque τ, vertical acceleration $\ddot{z}$, and CoP x_c, respectively. Feedback control of the desired model control U^d and measured model control U^m were used to generate the required corrective joint torques for tracking. For the NMPC models that do not utilize the hip or variable height strategies, the hip and knee controller regulated the torso pose and hip height to the desired resting pose. Additional ankle torque modulated by f_{heel} prevented heel lift during large disturbances.

For tracking, the reduced order model received state measurements from the robot model. The robot horizontal CoM position relative to the ankle joint and hip height were used as the CoM position x and z of the reduced order models while the robot torso angle relative to the ground frame was the flywheel angle for the reduced order models. The vertical CoM position of the robot was not used to remove variable height corrective behavior induced by hip rotations. Other measurements used were CoP position x_c and the vertical acceleration $\ddot{z}$. The measured raw x_c and $\ddot{z}$ signals exhibited some spikes due to the contact model, and we applied a low-pass filter with a cutoff frequency of 17.5 Hz and 12 Hz, respectively, to mitigate their effect on feedback control.

F. Push Recovery Simulation

In the push recovery simulations for the reduced order models and the simple balancing robot, we modeled push disturbances as a constant horizontal force applied for 0.1 s. We applied a range of push force magnitudes until the system failed to recover from the disturbance. For the reduced order model simulation, we applied the force to the COM, and for the one legged robot, we applied the force to the hip joint. To find the maximum recoverable push, both systems experienced increasing pushes in increments of 20 N that were refined near failure. This procedure resulted in an average total of 28 pushes for the reduced order models and 24 pushes for the robot models.

To evaluate push recovery performance, we recorded the capture point which represents the point on the ground the CoP needs to be positioned for natural LIP dynamics to bring the system back to rest [9]. The capture point ξ is given by

$$\xi = x + \frac{\dot{x}}{\omega} \tag{7}$$

where $\omega = \sqrt{g/z}$. The capture point has been used as metric of stability and to determine when to switch between different balancing strategies [2]. Smaller capture point values indicate better performance because less action is needed to bring the system to rest. We compared the maximum absolute value of the capture point from each simulation.

To compare how each balancing strategy was used over the range of disturbances, we compared relative usage of each component of the NMPC control U. Each control component x_c, τ, and $\ddot{z}$ corresponded to an individual balancing strategy: ankle, hip, and variable height, respectively. We defined c^j as the relative contribution of the j^{th} component of the control signal $\mathbf{u}^j$, representing $\mathbf{x_c}$ τ, or $\ddot{\mathbf{z}}$, generated by the NMPC:

$$c^j = \frac{\sum_i \tilde{u}_i^{j^2}}{C} \tag{8}$$

TABLE V: Maximum recoverable push magnitude for each reduced order model in push recovery simulations of the model dynamics and on a simple one legged balancing robot.

Reduced Order Model	Model [N]	Robot [N]
LIP	490	421
LIPPFW	566	463
VHIP	511	454
VHIPPFW	586	478

where $\tilde{u}_i^j = u_i^j / u_{\max}^j$ is the i^{th} element in the control sequence $\mathbf{u}^j$ normalized to its control limit $u_{\max}^j$ and C is the sum of all normalized controls.

III. Results

For the simulations of the reduced order models using NMPC, we found that the VHIPPFW model could recover from the largest push force of 586 N followed by the LIPPFW at 566 N, then the VHIP at 511 N, and finally the LIP at 490 N. We observed increased performance when additional balancing strategies were available to the model both in terms of maximum capture point (Fig. 4) and the phase of CoM (Fig. 5). Models that included the hip strategy (LIPPFW and VHIPPFW) had the largest impact, reducing the maximum capture point by 5.7% and 5.4% on average compared to LIP and VHIP, respectively. Strategies that included variable height (VHIP and VHIPPFW) reduced the maximum capture point by 1.3% and 1.0% compared to LIP and LIPPFW, respectively. The performance differences were most evident in the phase plots with the CoM phase encircling the smallest area with the VHIPPFW, followed by the LIPPFW, VHIP, and LIP.

Like the reduced order model simulations, the largest push disturbance that the one legged balancing robot could recover from was achieved with the VHIPPFW at 478 N (see Fig. 10 for the time-lapse of a representative simulation). The next best were the LIPPFW, VHIP and LIP which had a maximum recoverable push disturbance of 463, 454 and 421 N, respectively. The maximum capture points $\xi_{\max}$ from the robot demonstrated less delineation among the strategies than the reduced order model results (Fig. 6). For disturbances less than 400 N, the VHIPPFW had the lowest capture point followed by LIPPFW, VHIP and LIP. For disturbances exceeding 400 N, the VHIP capture point was lowest. The addition of the hip strategy in LIPPFW and VHIPPFW reduced the capture point by 2.9% and 3.2% compared to LIP and VHIP models, respectively, whereas the addition of the variable height strategy in the VHIP and VHIPPFW reduced the maximum capture point by 2.2% and 3.3% compared to the LIP and LIPPFW models, respectively. The CoM phase plot for the one legged robot also showed a similar performance with the VHIPPFW encircling the smallest area (Fig 7). The robot models that used the hip strategy had the largest impact on reducing CoM excursions but also exhibited overshoot on the return to rest.

From the maximum recoverable disturbances for simulations of the reduced order model dynamics and simple one legged balancing robot (summarized in Table V), we

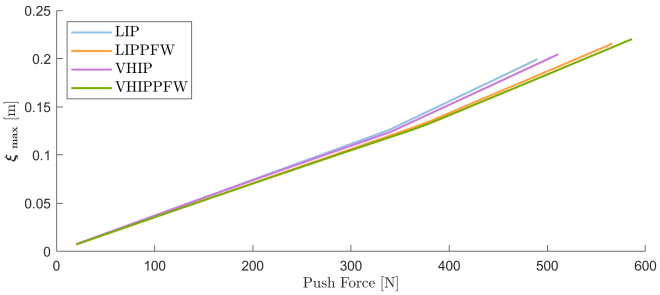

Fig. 4: Maximum capture point $\xi_{\max}$ experienced for reduced order model NMPC simulations.

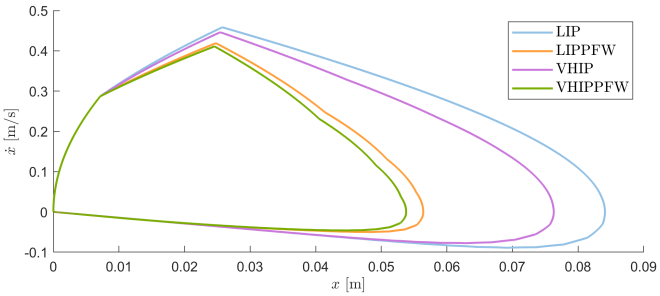

Fig. 5: Comparison of the CoM phase plots during push recovery simulation of the reduced order models with push disturbance of 400 N for 0.1 s.

observed that the robot was unable to reject the same disturbances as the reduced order models, dropping its performance by 15.5% on average. The hip was less effective in the robot models with the largest drop of 18.3% in the models that used the hip strategy.

The unified VHIPPFW model took advantage of all three strategies, and the contributions of each strategy changed with push magnitude (Fig. 8 for the reduced order models, Fig. 9 for the robot model). While the ankle strategy could be applied throughout the recovery, the hip and variable height strategies were constrained by limits on θ and z, respectively, so they were primarily deployed at the onset of the disturbance (Fig. 11). The ankle strategy was the dominant strategy over the hip and variable height strategies, representing greater than 77.9% (reduced order model) and 80.1% (robot) of the relative control contribution over the whole range of push disturbances. The contribution of the ankle strategy was the greatest at smaller disturbances and dropped as the other balancing strategies were adopted as push disturbance increased. The hip strategy contribution broadly changed in inverse proportion to the ankle strategy, accounting for an average of 10.8% (reduced order model) and 12.8% (robot) of control. In contrast to the hip strategy, the variable height strategy generally exhibited a low but steady increase in contribution as push magnitude increased and accounted for an average of 3.6% (reduced order model) and 2.6% (robot) of the total cost.

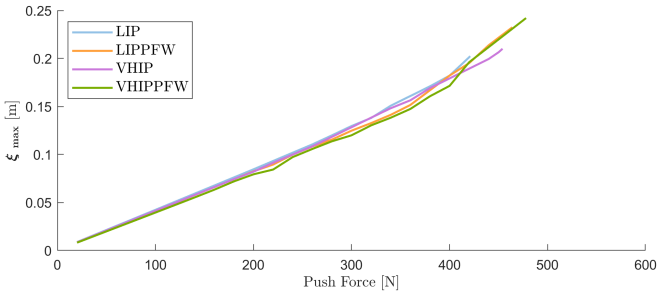

Fig. 6: Comparison of the maximum capture point ξ_{max} experienced for the simple one legged balancing robot simulations.

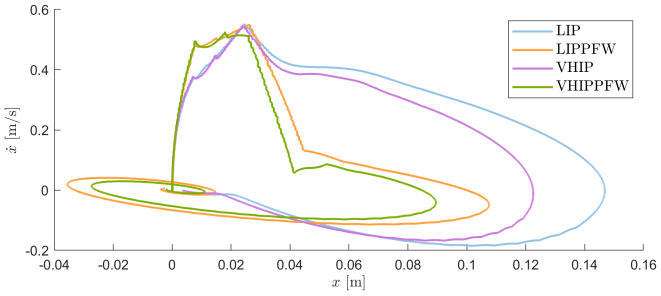

Fig. 7: Comparison of the CoM phase plots during push recovery simulation of the simple one legged balancing robot with push disturbance of 400 N for 0.1 s.

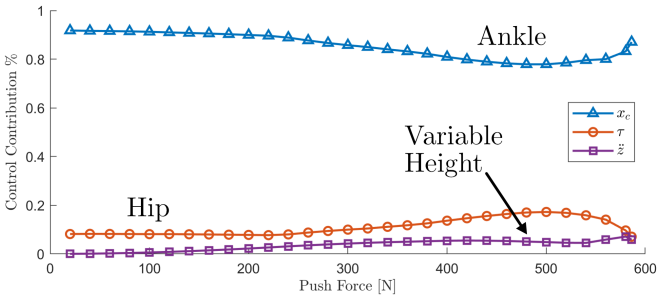

Fig. 8: Percent contribution of each control strategy in VHIPPFW reduced order model using the normalized control cost.

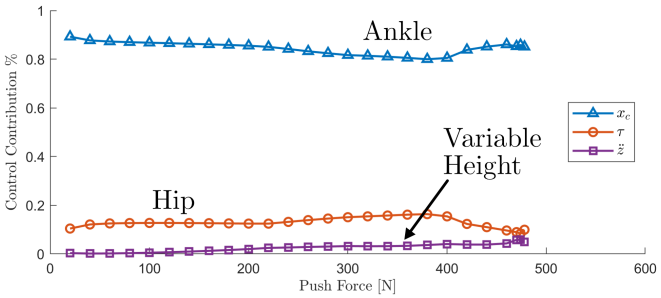

Fig. 9: Percent contribution of each control strategy in the robot implementation of the VHIPPFW reduced order model using the normalized control cost.

IV. Discussion

We simulated push recovery on four different reduced order standing balance models, including a new unified standing balance model VHIPPFW. We tested both reduced order models and a simulated one legged robot. For both systems, the VHIPPFW was able to recover from largest disturbances and had the lowest maximum capture point. Both VHIPPFW systems also exhibited similar progressions of control contribution with push disturbances. We observed that the ankle was the primary mechanism for balance for all push magnitudes. When the ankle strategy exhibited decreased contributions at larger pushes, the hip and variable height strategies increased to compensate. Between the hip and the variable height strategies, the hip had the largest effect on improving overall performance.

We observed a drop in performance between the reduced order models and its simulated robot implementation. The drop in performance was likely due to differences between the reduced order models and full body system. These issues are evident from the full body controller's ability to track NMPC control, such as the lag between desired and measured values for CoP and vertical accelerations (Fig. 11).

The inability to quickly reach the desired CoP values reduces the ankle strategy's efficacy on all robot models and highlights the limitations of a rigid foot. With a compliant or multi-linked foot, the shape of the foot could be altered to better concentrate the CoP at the edge of the base of support. Since LIP dynamics rely on the difference between the CoM and the CoP, any reduction in CoP tracking would limit recovery performance. The effectiveness of the hip strategy was also reduced in the one legged robot. Changes in hip angle could position the robot CoM outside the base of support, leading to failure. The coupling between the CoM position and torso angle was also the probable cause for the overshoot observed on the one legged robot when returning to the rest position (see Fig. 7). Furthermore, we only considered a momentum wheel with fixed inertia, whereas configuration dependent inertia would be more relevant to real systems.

The inclusion of additional strategies led to greater computational complexity. VHIPPFW required the longest processing time, averaging 1.7 times more than the next complex model LIPPFW and 5.3 times more than the simplest model LIP. The current NMPC controllers for LIPPFW and VHIPPFW models cannot be solved online as the processing time exceeded the NMPC sample time. Further tuning of the NMPC by either reducing the prediction horizon, using sub-optimal solutions, or improving processing capability could be explored to allow for practical implementation. Similar to balance during stepping [17], variable height has a relatively minimal contribution to standing balance and could be removed at a small cost to performance.

Despite these limitations, the availability of more balancing strategies in the unified model resulted in the best recovery performance for both the reduced order model and the robot simulations. The unified controller was able to

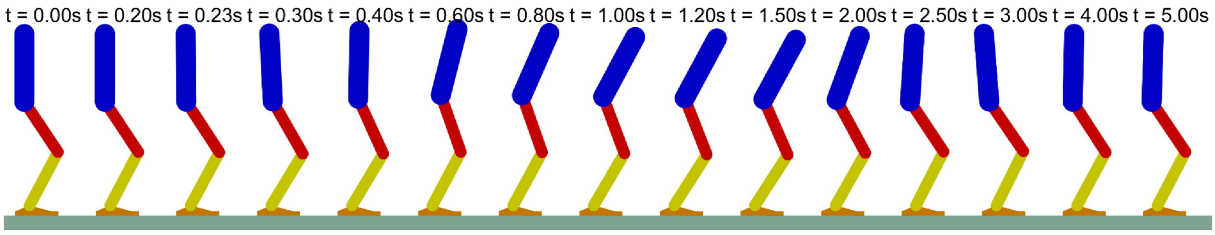

Fig. 10: Time-lapse of the simple one legged balancing robot using the VHIPPFW NMPC subject to a 478 N push disturbance sustained for 0.1 s. The push onset occurred after 0.2 s into the simulation.

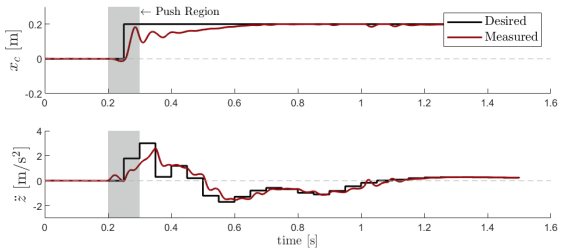

Fig. 11: Desired (black) and measured (red) NMPC control signals for CoP and vertical acceleration of VHIP model in response to a push disturbance of 454 N applied for 0.1 s on the one legged robot.

take advantage of each strategy as needed to respond to pushes of various magnitudes. In the selection of balancing strategies, the controller displayed human-like preferences, decreasing the use of the ankle strategy while increasing use of the hip strategy with larger pushes. Our next steps are to implement the robot controller onto a physical robot leg currently under development. The promising results of the unified controller in simulation indicate that enabling legged robots to have access to all three balance strategies may lead to improved ability to successfully recover from larger push disturbances, increasing robot robustness and utility in real-world situations.

V. Acknowledgments

Funding was provided by Ingenuity Labs Research Institute at Queen's University and the Natural Sciences and Engineering Research Council of Canada (NSERC).

References

[1] C. McGreavy, K. Yuan, D. Gordon, K. Tan, W. J. Wolfslag, S. Vijayakumar, and Z. Li, "Unified push recovery fundamentals: Inspiration from human study," in *Proc. 2020 IEEE Int. Conf. Robotics and Automation*, 2020.

[2] B. Stephens, "Humanoid push recovery," in *2007 7th IEEE-RAS International Conference on Humanoid Robots*, 2007, pp. 589–595.

[3] A. D. Kuo, "An optimal control model for analyzing human postural balance," *IEEE Trans Biomed Eng*, vol. 42, no. 1, pp. 87–101, 1995.

[4] Z. Aftab, T. Robert, and P.-B. Wieber, "Ankle, hip and stepping strategies for humanoid balance recovery with a single Model Predictive Control scheme," in *2012 12th IEEE-RAS International Conference on Humanoid Robots*, 2012, pp. 159–164.

[5] B. J. Stephens and C. G. Atkeson, "Push Recovery by stepping for humanoid robots with force controlled joints," in *2010 10th IEEE-RAS International Conference on Humanoid Robots*, 2010, pp. 52–59.

[6] C. G. Atkeson and B. Stephens, "Multiple balance strategies from one optimization criterion," in *2007 7th IEEE-RAS International Conference on Humanoid Robots*, 2007, pp. 57–64.

[7] Y.-M. Chen and M. Posa, "Optimal Reduced-order Modeling of Bipedal Locomotion," in *2020 IEEE International Conference on Robotics and Automation*, 2020, pp. 8753–8760.

[8] S. Kajita, F. Kanehiro, K. Kaneko, K. Yokoi, and H. Hirukawa, "The 3D linear inverted pendulum mode: a simple modeling for a biped walking pattern generation," in *2001 IEEE/RSJ International Conference on Intelligent Robots and Systems*, 2001, pp. 239–246.

[9] J. Pratt, J. Carff, S. Drakunov, and A. Goswami, "Capture point: A step toward humanoid push recovery," in *2006 6th IEEE-RAS International Conference on Humanoid Robots*, 2006, pp. 200–207.

[10] B. J. van Hofslot, R. Griffin, S. Bertrand, and J. Pratt, "Balancing Using Vertical Center-of-Mass Motion: A 2-D Analysis From Model to Robot," *IEEE Robotics and Automation Letters*, vol. 4, no. 4, pp. 3247–3254, 2019.

[11] T. Koolen, M. Posa, and R. Tedrake, "Balance control using center of mass height variation: Limitations imposed by unilateral contact," in *2016 IEEE-RAS 16th International Conference on Humanoid Robots (Humanoids)*, 2016, pp. 8–15.

[12] S. Kajita, F. Kanehiro, K. Kaneko, K. Fujiwara, K. Harada, K. Yokoi, and H. Hirukawa, "Biped walking pattern generation by using preview control of zero-moment point," in *2003 IEEE International Conference on Robotics and Automation*, vol. 2, 2003, pp. 1620–1626 vol.2.

[13] R. R. Neptune and C. P. McGowan, "Muscle contributions to whole-body sagittal plane angular momentum during walking," *Journal of Biomechanics*, vol. 44, no. 1, pp. 6–12, 2011.

[14] S. Park, F. B. Horak, and A. D. Kuo, "Postural feedback responses scale with biomechanical constraints in human standing," *Exp Brain Res*, vol. 154, no. 4, pp. 417–427, 2004.

[15] F. B. Horak, "Postural orientation and equilibrium: what do we need to know about neural control of balance to prevent falls?" *Age Ageing*, vol. 35, pp. ii7–ii11, 2006.

[16] S. Caron, A. Escande, L. Lanari, and B. Mallein, "Capturability-Based Pattern Generation for Walking With Variable Height," *IEEE Transactions on Robotics*, vol. 36, no. 2, pp. 517–536, 2020.

[17] M. Posa, T. Koolen, and R. Tedrake, "Balancing and Step Recovery Capturability via Sums-of-Squares Optimization," in *Robotics: Science and Systems*, 2017.

[18] T. Koolen, T. de Boer, J. Rebula, A. Goswami, and J. Pratt, "Capturability-based analysis and control of legged locomotion, Part 1: Theory and application to three simple gait models," *The International Journal of Robotics Research*, vol. 31, no. 9, pp. 1094–1113, 2012.

[19] D. A. Winter, *Biomechanics and motor control of human movement*, 4th ed. Hoboken, N.J: Wiley, 2009.

[20] Steve Miller, "Simscape Mulitbody Contact Forces Library," 2021. [Online]. Available: https://github.com/mathworks/Simscape-Multibody-Contact-Forces-Library/releases/tag/21.2.5.0

[21] MathWorks Student Competitions Team, "MATLAB and Simulink Robotics Arena: Walking Robot," 2021. [Online]. Available: https://github.com/mathworks-robotics/msra-walking-robot